PCCP

Accepted Manuscript

ROYAL SOCIETY OF CHEMISTRY

www.rsc.org/pccp

ARTICLE TYPE www. rsc.org/xxxxxx | XXXXXXXX

Stability of Two-Dimensional PN Monolayer Sheets and Their Electronic Properties

ShuangYing Ma[a], Chaoyu He[a], L. Z. Sun[b†], Haiping Lin[c], Youyong Li[c], and K. W. Zhang[a ‡]

Received Xth XXXXXXXXXX 20XX, Accepted Xth XXXXXXXXX 20XX
First published on the web Xth XXXXXXXXXX 200X
DOI: 10.1039/b000000x

Three two-dimensional phosphorus nitride (PN) monolayer sheets (named as α-, β-, and γ-PN, respectively) with fantastic structures and properties are predicted based on first-principles calculations. The α-PN and γ-PN are buckled structure, whereas β-PN shows puckered characteristics. Their unique structures endows these atomic PN sheets with high dynamic stabilities and anisotropic mechanical properties. They are all indirect semiconductors and their band gap sensitively depends on the in-plane strain. Moreover, the nanoribbons patterned from these three PN monolayers demonstrate remarkable quantum size effect. Particularly, the Zigzag α-PN nanoribbon shows size-dependent ferromagnetism. Their significant properties show potential in nano-electronics. The synthesis of the three phases of PN monolayer sheets is proposed theoretically, which is deserved to further study in experiments.

1 Introduction

The synthesis of Graphene and its excellent properties[1] promote the research of low-dimensional nano-materials into two-dimensional (2D) epoch[2–4]. In past decade, considerable efforts have been pursued on the discovery of 2D materials beyond graphene[1] such as hexagonal BN[1,5], dichalcogenide[1,6], group IV[7–10], II-VI[11–13], and III-V compounds[14–16] metastable monolayer. Recently, as representatives of group V, the monolayer composed purely of single element of phosphorene[17–20], arsenene[21,22], and antimonene[21], were theoretically predicted and some of them were synthesized in experiment. Importantly, few-layer black phosphorus and arsenene show high carrier mobility[23,24], which endows them with great potential in future nanoelectronics. However, up to date, as the representative of group V-V monolayer compounds, the monolayer counterpart of phosphorus nitride compounds has not been reported yet even though some three-dimensional (3D) phosphorus nitride compounds crystals had been found several decades ago.

To our knowledge, the only synthesized phosphorus nitride crystal is P_3N_5 with a variety of pressure-dependent phases[25–30]. In particular, all of the phases are only stable under high pressure except for its α phase. A previous DFT calculation indicated that the α phase transforms into γ phase under around 6 GPa, and further into δ phase with Kyanite-like structure under about 43 GPa[30]. Recently, two new phases PN_3 and PN_2 were theoretically predicted. They are also only stable under high pressures[31]. The question is why so many PN phases can only exist under high pressures except for α-P_3N_5. Although Raza et al.[31] pointed out that the instability of PN_3 results from the existing of N-N units which tends to form N_2 pair, there is not N-N bond in other PN phases. Through structural analysis, we find that the coordination number of P and N atom in these PN phases is approximately proportional to the stable pressure of corresponding PN phase. For example, α-P_3N_5 is stable at ambient pressure[31], whose coordination number of P and N atom $\leq$ 4 and 3, respectively; whereas the coordination number of P and N atom is 6 and 4, respectively for PN_2 phase whose stable pressure is above 200 GPa[31]. Therefore, we extrapolate that to obtain a kind of stable phosphorus nitride compounds crystal under lower or even ambient pressure the coordination number of P and N atom $\leq$ 4 and 3, respectively. Many works had been done on phosphorus nitride compounds molecules such as cyclic phosphazenes with 1:1 mole fraction of P and N[25,32]. The results indicated that cyclic phosphazenes are surprisingly stable, and their stability is insensitive to their planar or puckering configuration[32]. Meanwhile, since N and P atoms are favorable to form three coordinated 2D systems, such as h-BN monolayer[1,5] and phosphorene[17–20], adopting hexagonal three coordinated PN units with 1:1 mole fraction between P and N is hoping to construct 2D PN monolayer nano materials.

In this paper, using first-principles method we propose three stable 2D monolayer phases of phosphorus nitride named as α-, β-, and γ-PN. They are all indirect band gap semiconduc-

[a] *School of Physics and Optoelectronics, Xiangtan University, Xiangtan 411105, China. E-mail: kwzhang@xtu.edu.cn*
[b] *Hunan Provincial Key laboratory of Thin Film Materials and Devices, School of Material Sciences and Engineering, Xiangtan University, Xiangtan 411105, China. E-mail: lzsun@xtu.edu.cn*
[c] *Institute of Functional Nano & Soft Materials (FUNSOM), Soochow University, Suzhou 215123, China.*

tor with low-buckled honeycomb structures. Their band gaps can be effectively tailored by in-layer strain, patterning, and multi-layer stacking. Meanwhile, we propose PN compound closely similar to graphite based on the 2D monolayer PN obtained in our present work due to the weak inter-layer interaction for the three monolayer PN.

2 Computational Details

We performed first-principles calculations based on density functional theory as implemented in the VASP code[33,34] to investigate the equilibrium structures, stability, and electronic properties of α-, β-, and γ-PN. The electron-electron interaction was treated with a generalized gradient approximation (GGA) proposed by Perdew, Burke, and Ernzerhof (PBE)[35]. Projector-augmented wave (PAW)[36,37] method was used for describing interaction between valence electrons and core. A kinetic-energy cutoff of 400 eV was selected for the plane wave basis set. To avoid the interaction between neighboring images a vacuum space of 15 Å perpendicular to the plane of the 2D systems was set. The Brillouin zone was sampled using $13\times13\times1$ Monkhorst-Pack k-point scheme. The total energy convergence criterium was 10^{-5} eV. All systems were fully relaxed until the residual Hellmann-Feynman forces were smaller than 0.01 eV/Å. The energetic stability of the systems was evaluated by comparing their formation enthalpy[38,39] ΔG defined as,

$$\Delta G = E_{coh} - \sum \chi_i \mu_i. \quad (1)$$

The term E_{coh} is the cohesive energy per atom of the specific PN phase considered here, χ_i (i denote P, N) is the molar fraction of the groups and they obey the rule of $\sum \chi_i = 1$. μ_i is the chemical potential of the constituents at a given state. We chose μ_P as the cohesive energy per atom of pristine monolayer black phosphorene; and μ_N was taken as the binding energy per atom of N_2 molecule. Considering the cohesive energy ΔE is useful to evaluate the probability to form vacancy and other defects, similar to that in graphene and silicene[40], the ΔE of the systems was also calculated. The cohesive energy ΔE is defined as,

$$\Delta E = (E_{TOT} - n_N E_N - n_P E_N)/n_N + n_P. \quad (2)$$

The term E_{TOT} is the total energy of a specific PN phase considered here, n_N and n_P is the number of N and P atoms in the unit-cell of specific PN phase, respectively. E_N is one half of the total energy of N_2 molecule and E_P is total energy per atom of monolayer black phosphorene. To verify the stabilities of the three phases, besides phonon spectrum, ab initio molecular dynamics (AIMD) simulations were also performed.

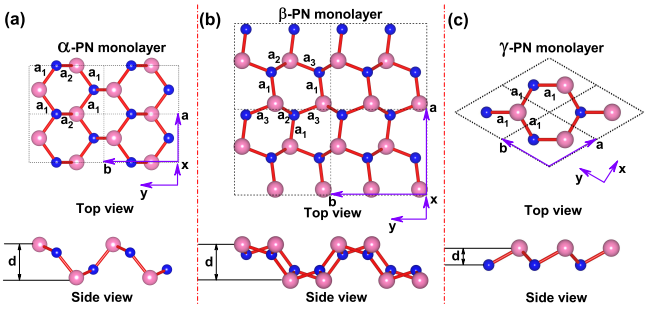

Fig. 1 (a), (b), and (c) respectively are top and side view of 2×2 supercell of optimized structures of α-, β-, and γ-PN monolayers. The balls in blue and pink represent nitrogen and phosphorus atoms, respectively. d is the thickness of the quasi-2D monolayers. a_1, a_2, and a_3 stand for nonequivalent bond of the three phases.

3 Results and Discussions

With the restriction as mentioned above:(i) 1:1 mole fraction between N and P; (ii) two dimensional hexagonal configuration, we propose three two-dimensional phosphorus nitride (PN) monolayer sheets named as α-, β-, and γ-PN, respectively. The optimized structures of the three phases are shown in Fig. 1. The structural parameters of the three PN sheets are listed in Tab. 1. Due to the different local environment of P and N atoms, there are two and three non-equivalent bond lengths for α and β phases, respectively. The bond length between P and N atom of the three phases is around 1.725∼1.821 Å. There are respectively four and eight atoms in the rectangular unit cell of α- and β-PN, and two atoms in hexagonal unit cell of γ-PN. Each atom in the three phases shows threefold coordination. All of them show non-planar configuration with a thickness about 0.861∼1.897 Å due to the phosphorus prone to form a tetrahedral configuration with its three nitrogen neighbors. However, as for α- and β-PN each nitrogen and its three nearest neighbor (NN) phosphorus are nearly on an identical plane. The formation enthalpy as listed in Tab. 1 shows that α and β phases are more stable than that of γ phase. The results indicate that as for PN monolayer phase the P and N atoms are energetically favorable to form sp^3 and sp^2 hybridized configuration, respectively. The structural difference of the three monolayer PN sheets can be ascribed to the different way of connecting tetrahedral coordinated phosphorus atom with its three NN nitrogen atoms. The side view of the β-PN shows ridge-like configuration that is, to some extent, analogous to that of α- and δ-phosphorene. α- and γ-PN are similar to the configuration of β- and γ-phosphorene, respectively.

The formation enthalpy (ΔG) of the three PN phases as shown in Tab. 1 is negative suggesting their possible existence in reality. The most stable phase is α-PN which is 40

Table 1 The lattice constants (a and b), nonequivalent bond length between phosphorus and nitrogen atom (a_1, a_2 and a_3), thickness of the monolayers d, space group (SG), formation enthalpy (ΔG defined by equation 1) and cohesive energy (ΔE defined by equation 2) of α-, β-, and γ-PN monolayers.

	$\vec{a}$(Å)	$\vec{b}$(Å)	a_1(Å)	a_2(Å)	a_3(Å)	SG	d(Å)	ΔG(eV)	ΔE(eV/atom)
α-PN	2.703	4.190	1.725	1.821		Pmn21	1.892	-0.40	-4.407
β-PN	4.516	5.070	1.749	1.797	1.737	Pca21	1.897	-0.36	-4.362
γ-PN	2.756	2.756	1.809	1.809		P3m1	0.861	-0.08	-4.086

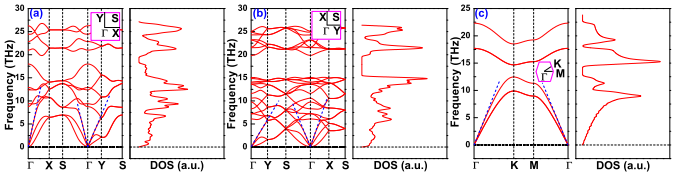

Fig. 2 Phonon band structures and density of states of (a) α-PN,(b) β-PN, and (c) γ-PN, respectively.

meV more stable than that of β-PN. To further confirm their dynamic stability, we calculated their phonon band structures and phonon density of states[41]. The phonon spectra are shown in Fig. 2. There are no negative frequencies and states in the phonon band structure and phonon density of states, confirming the dynamic stability of the three PN sheets. The highest frequency of α-, β-, and γ-PN, as an indication of the robustness of the P-N bonds, reaches up to 26.8, 26.0, and 22.3 THz, respectively, which to some extent indicates their relative stability. The higher frequency of longitudinal optical modes manifests a larger in-plane rigidity. The results indicate that the rigidity sequence is $\alpha > \beta > \gamma$. To further check their thermodynamic stabilities, ab initio molecular dynamics (AIMD) calculations were performed. In the calculations, relatively large supercells (5×4×1, 1×3×3, and 4×4×1 for α-, β-, and γ-PN, respectively), NVT ensemble, and 1 fs time step were adopted. The results indicate that the three PN sheets can sustain their original structures at least 6 ps under 800 K. In particular, the α-PN even does not show structural instability during a 6 ps AIMD simulation at 1600 K. The above results give firm evidence that the three PN sheets are stable enough to be observed in the experiments.

We then investigate the slopes of the longitudinal acoustic branches near Γ point, which corresponds to the speed of sound and in-plane stiffness. According to the results in Fig. 2 (a), the sound velocity along the Γ-X orientation of α-PN ($v_s^{\Gamma-X}$=11.2km/s) is nearly two times larger than that along Γ-Y direction ($v_s^{\Gamma-Y}$=5.3 km/s). The results indicate that for α-PN, the stiffness is anisotropic that along $\vec{a}$ orientation is much larger than that along $\vec{b}$ direction. If a finite compression stress is applied along $\vec{a}$ direction the bond bending is prevail to bond stretching due to the lower energy cost for the former one. Similar results can be found for β-PN. The velocity of sound along the Γ-Y direction of β-PN ($v_s^{\Gamma-Y}$=6.0 km/s) is nearly the half of that along Γ-X orientation ($v_s^{\Gamma-X}$=10.54 km/s). Accordingly, the stiffness along $\vec{b}$ orientation is much lower than that along $\vec{a}$ direction. Considering the structure equivalence of γ-PN along $\vec{a}$ and $\vec{b}$ axis of unit cell, we only present the velocity of sound along one crystal axis direction. Corresponding to the reciprocal space, the direction is along Γ-M. The results indicate that the $v_s^{\Gamma-M}$ is 6.89 km/s. Meanwhile, the velocity of sound along the diagonal direction of crystal axis $\vec{a}$ and $\vec{b}$, namely, $v_s^{\Gamma-K}$=7.06 km/s, which is closed to that along crystal axis direction. The results derive from the isotropic structure characteristics of γ-PN.

As shown in Fig. 3 (a), (c), and (e), the DFT-PBE calculations show that the single-layer α-PN, β-PN, and γ-PN are all indirect band gap semiconductor with the energy gaps of 1.638, 2.197, and 1.800 eV, respectively. Considering the fact that PBE functional always underestimates the band gap of semiconducting materials, we also use HSE06 functional[42,43] to study their energy gaps. The revised energy-gap values are 2.689, 3.282, and 2.532 eV, respectively. Partial density of states (PDOS) for the three phases are shown in Fig. 3 (b), (d), and (f). The results indicate that the valence-band maximum (VBM) of α-PN is mainly contributed by p_z states of N and P atoms and s orbital of P atoms; for β-PN, the VBM primarily derives from p_z orbital of N and P atoms and s orbital of P atoms; the VBM of γ-PN is largely determined by p_z+p_x orbitals of N and P and s orbital of P atoms. Below VBM, the p and s orbitals of N and P atoms show similar electronic resonance, suggesting strong hybridization and charge transfer between N and P atom. The charge transfer between N and P atom can be clearly verified by the charge density difference as shown in Fig. 4 (a), (b), and (c). The results show that electrons transfer from P to N atom and mushroom-shaped electron cloud is generated for P atom due to charge redistribution. Bader charge analysis[44,45] reveals the transferred net charge for α-, β-, and γ-PN is 3.257, 3.221 and 3.110e, respectively, indicating obvious ionic bond characteristics between P and N atom.

Based on the three 2D monolayer PN sheets proposed above, we investigate the 3D PN systems analogous to graphite through stacking of them. Fig. S1 shows the optimized geometries with different stacking orders for the 3 kinds of multilayer PN phases. The minimum interlayer distance for multilayer PN phases is about 4.343 Å, which is at least 0.848 Å larger than that of AA stacking black Phosphorene. Moreover, except for a small minish of the lattice constants and bond length for multilayer γ-PN, the structure parameters of the other two multilayer PN phases are nearly unchanged. The band gap of the three multilayer phases as shown in Fig. 5

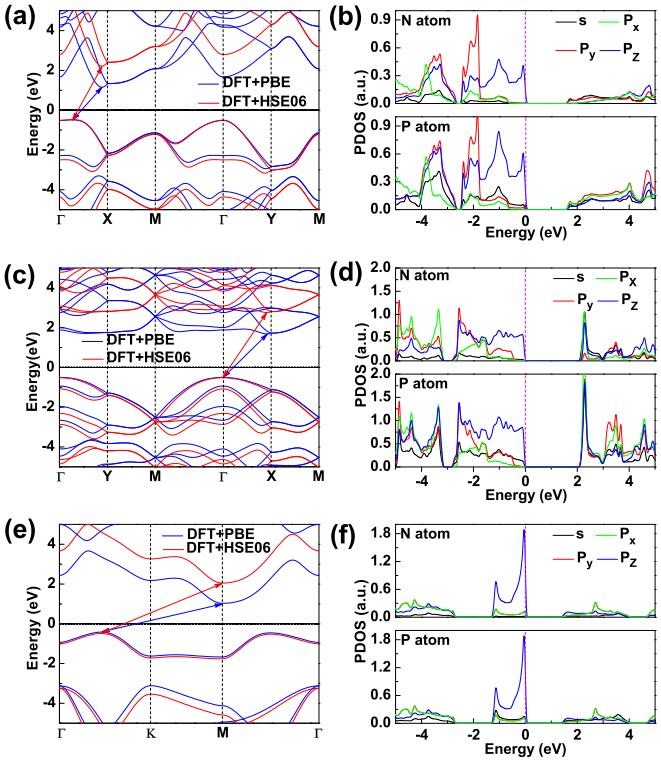

Fig. 3 (a), (c), and (e) respectively are the band structures of α-PN, β-PN, and γ-PN. (b), (d), and (f) correspond to partial density of states of α-, β-, and γ-PN, respectively.

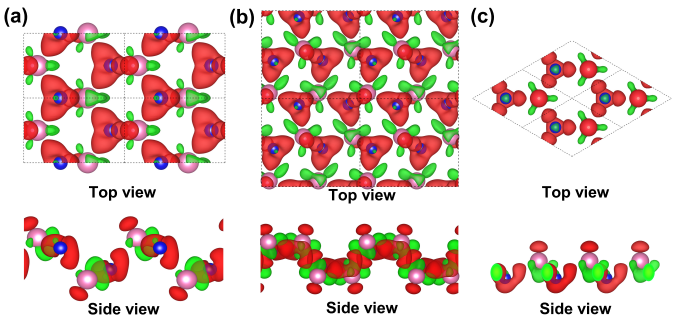

Fig. 4 Charge density difference of α-PN (a), β-PN (b), and γ-PN (c), respectively. The isosurface is 0.018 e/Å^3). The red and green color stands for charge increase and decrease region corresponding to isolated atoms, respectively.

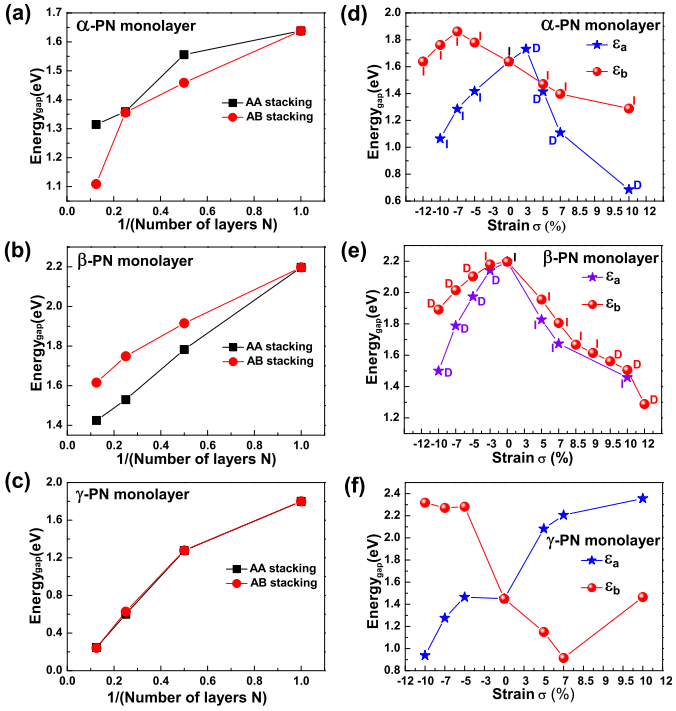

Fig. 5 (a), (b), and (c) respectively are the band gap of α-, β-, and γ-PN in function of the stacking thickness. (d), (e), and (f) shows the band gap in function of strain for α-, β-, and γ-PN, respectively. I and D denote the indirect and direct band gap semiconductor, respectively.

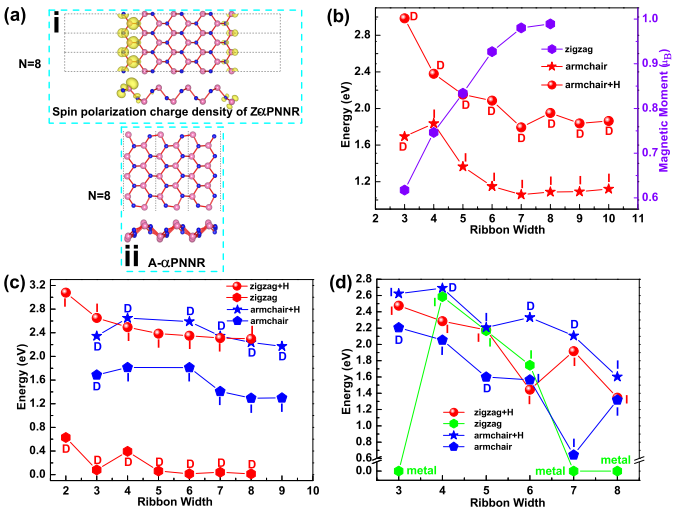

Fig. 6 Panel i and ii in (a) are the DFT-optimized structures of Z-αPNNR and A-αPNNR with the width of N=8, respectively. The yellow color of panel i is the spin polarized charge density with isosurface of 0.005e/Å^3. (b), (c), and (d) are the band gap of nanoribbon as a function of ribbon width (N) for α-PN, β-PN, and γ-PN, respectively. The letter I and D in the figures denote the indirect and direct semiconductor, respectively. The symbol "+H" means the edges of the nanoribbon is passivated by H atoms.

(a), (b), and (c) is approximately inversely proportional to the number N of stacking layer. Meanwhile, the dependence of the band gap on the stacking layer is sensitive to the stacking order except for the γ phase. Although the van der Waals interaction between layers will result in the energy level splitting and the strength of the splitting is proportional to N, the band-structure of multilayer PN are roughly similar to their corresponding monolayer PN phases, as shown in Fig. S2. In contrast to the case of phosphorene whose energy gap decreases with the increase in N is the reason of wave function overlap between layers, the wave function overlap of multilayer PN is slight (the results are shown in Fig. S3). The results indicate that the dependence of the band gap on the N of multilayer PN derives from van der Waals interactions between layers due to its larger interlayer distance. For α-PN, the band gap can be tuned from 1.64 eV (monolayer) to 1.31 (AA stacking, N=8) or 1.11 eV (AB stacking, N=8). As for β-PN, its band gap changes from 2.20 eV (monolayer) to 1.42 eV (AA stacking, N=8) or 1.62 eV (AB stacking, N=8). The band gap of γ-PN for AA and AB stacking is nearly degenerate as shown in Fig. S2 due to its larger interlayer distance. The tunable band gap ranges from 1.80 eV (monolayer) to 0.24 eV (N=8). The dependence of the band gap on the thickness produces the three PN phases show wide range adjustability of their electronic properties.

Another intriguing issue is the sensitive dependence of the band gap of the three PN phases on in-plane strain exerted along two axial directions, as shown in Fig. 5 (d), (e), and (f) for α-PN, β-PN, and γ-PN, respectively. Considering the un-planar feature of the three phases, the external strain -12%$\sim$12% can be achieved without large energy cost similar to that of phosphorene [17,19]. α-PN is an indirect-band-gap semiconductor under zero strain. When apply strain along axial vector $\vec{a}$, its energy gap decreases regardless of compression or tension. Meanwhile, α-PN transforms into a direct band gap semiconductor when the stretching strain increases to 3% from 0%. A detailed analysis on anteroposterior structural parameters indicates that the value of lattice constant a increases by 0.081 Å, while b reduces by 0.091 Å; its nonequivalent bond length a_1 increases by 0.024 Å but a_2 reduces by 0.007 Å. Moreover, the thickness d of α-PN increases by 0.009 Å. The deformation of the structure results in the indirect-direct transition of the band type of α-PN. Such band type change is suitable for the application of α-PN in optoelectronics. Considering the strain scope, it can be easily exerted on the system when α-PN is grown on substrate. The band structures of α-PN as shown in Fig. S4 (a) indicate that its VBM and CBM turn from original Γ-X line to Γ point as increasing of tensile strain along the a axis. When the σ is larger than 3% its band gap turns from indirect to direct one. The value of energy gap is also sensitive to the strain which is tuned from 1.638 eV at $\sigma = 0$ to 1.065 eV at $\sigma = -10\%$

and 0.686 eV at $\sigma = 10\%$. However, exerting stress along another lattice vector $\vec{b}$, whether compression or stretch, the band of α-PN remains its indirect type, as shown in Fig. S4 (b). The energy gap increases from 1.638 eV under $\sigma = -12\%$ to 1.861 eV under $\sigma = -7\%$, whereas the band gap decreases from 1.861 eV at $\sigma = -7\%$ to 1.288 eV at $\sigma = 10\%$. As for β-PN, its band gap decreases for both compressed and stretched strain along both cell vectors. By compressing along vector $\vec{b}$ or $\vec{a}$, the gap can be modified from 2.197 eV (at $\sigma = 0$) to 1.891 eV (along $\vec{b}$, for $\sigma = -10\%$) and 1.288 eV (along $\vec{b}$, for $\sigma = 12\%$) or 1.500 eV (along $\vec{a}$, for $\sigma = -10\%$) and 1.459 eV (along $\vec{a}$, for $\sigma = 12\%$). When the strain along $\vec{a}$, the system behaves as indirect and direct band gap semiconductor for stretch and compress strain, respectively. However, as for the strain being along $\vec{b}$, when the strain is larger than 9% and less than -5%, the system behaves as direct band gap semiconductor. The band structures of β-PN as shown in Fig. S5 indicate that the VBM of β-PN locates at Γ point under zero stain. The occurrence of the indirect-direct transformation is determined by the location of CBM. The CBM of β-PN under zero strain is close to X point. By applying suitable strain along a specific axis, the location of the CBM shifts from X to Γ point producing direct band gap semiconductor. From the point of view of structural parameters, we find that when the compression strain increases from $\sigma = 0\%$ to $\sigma = -3\%$ along $\vec{a}$ axis, both lattice constant a and b reduce by 0.135 and by 0.031 Å, which implies that β-PN behaves a negative Poisson's ratio during the compression process. Meanwhile, its nonequivalent bond length a_1, a_2 and a_3 respectively induces by 0.017, 0.002 and 0.002 Å, and the thickness d increases by 0.028 Å. The structure deformation results in the indirect-direct band type transition. When applying strain along b axis, the band type of β-PN also undergoes an indirect-direct transition when compression strain increases from $\sigma = -3\%$ to $\sigma = -5\%$. In the process, the lattice constant b reduces by 0.101 Å, however, a remains unchanged; its nonequivalent bond length a_1 increases by 0.002 Å while a_2 and a_3 respectively reduces by 0.001 and 0.002 Å. Moreover, the thickness d increases by 0.016 Å. As for γ-PN, its type of band gap is un-effected by the strain along both cell vector. When the strain is along vector $\vec{a}$ within the range of (10%, -10%), its energy gap change from 2.356 to 0.938 eV. However, when the strain is along vector $\vec{b}$, the response of the band gap to the strain is reversed to that along vector $\vec{a}$. Briefly summarized, external strain can effectively tune the band gap and even band type of the three 2D PN sheets. Such feature of the three systems is significant for their application in nanoelectronics and optoelectronics.

Patterning one dimensional (1D) nanoribbons from 2D system, such as graphene nanoribbon (GNR), is an effective approach to modulate the electronic properties of the 2D system and promote its applications. Considering the zigzag and armchair conventional notation of GNR, we take the zigzag and armchair edge PN nanoribbon (Z-PNNR and A-PNNR) as examples to study the electronic properties of 1D PNNR. Meanwhile, the number N of dimer lines across a specific nanoribbon is adopted to denote the width of nanoribbon with zigzag and armchair edges. For example, the Z- and A-αPNNR with the width N=8 is shown in panel i and ii of Fig. 6 (a), respectively. Both bared and H passivated edges of PNNR are considered in present work. Z-αPNNR and A-αPNNR can be fabricated by tailoring the layer along the $\vec{a}$ and $\vec{b}$ vector of α-PN, respectively. Our results indicate that among all PNNRs studied in our present work only the edges of Z-αPNNRs can not be passivated by H atoms. Such feature produces the Z-αPNNRs behave as ferromagnetic metal. As is shown in Fig. 6 (b), the magnetic moment of Z-αPNNRs increases linearly with the increase in the ribbon width. The magnetic moment saturates to 1 μB when N>6. The spin polarization charge density as shown in panel i of Fig. 6 (a) indicates that the spin coupling between two edges is ferromagnetic which is different from that of zigzag GNR. Meanwhile, the net magnetic moment is dominantly contributed by the edge N atoms and their nearest neighbor P atoms. A-αPNNRs are all semiconductors whether their edges are H-passivated or not, as shown in Fig. 6 (b). Moreover, their energy gap decreases with the increase in the ribbon width. Interestingly, by passivating the edges with H atoms, their band type transforms from indirect one into direct type. Meanwhile their energy gaps remarkably increase with the H passivation. In the case of β-PNNR, the situation of A-βPNNRs is very similar to that of A-αPNNRs. However, the edge-bared Z-αPNNRs are all direct-semiconductors. Their band type can be transformed into indirect one once the edges passivated by H atoms. The energy gap of Z-αPNNRs with bared edges tend to equilibrate around several meV when N >5. However, the H passivation significantly increases its band gap to around 2.4 eV. As for the case of γ-PNNRs, the H passivation can reverse the band type of A-γPNNRs when the band width is smaller than 8. The energy gap of all type of γ-PNNRs basically decreases with the increase in the ribbon width. When the ribbon width of bared edge Z-γPNNRs is smaller than 4 and larger then 8, the ribbon turn to metal.

Considering the successful synthesis of graphene, boron monolayer and especially silicene (which possesses buckled configuration that is similar to those of three PN phases) on metal surfaces[46–48], therefore, we here propose a possible growth method for the three monolayer PN sheets on Ag substrate by CVD method with cyclic phosphazenes. Although Raza et al.[31] indicated that extreme temperatures and pressures are required for synthesis many nitride compounds due to the high kinetic barrier to polymerisation derived from the high stability of nitrogen molecule at ambient pressure and the strong N≡N triple bond, we can overcome these difficulties through directly adopting some PN compounds molecules rather than

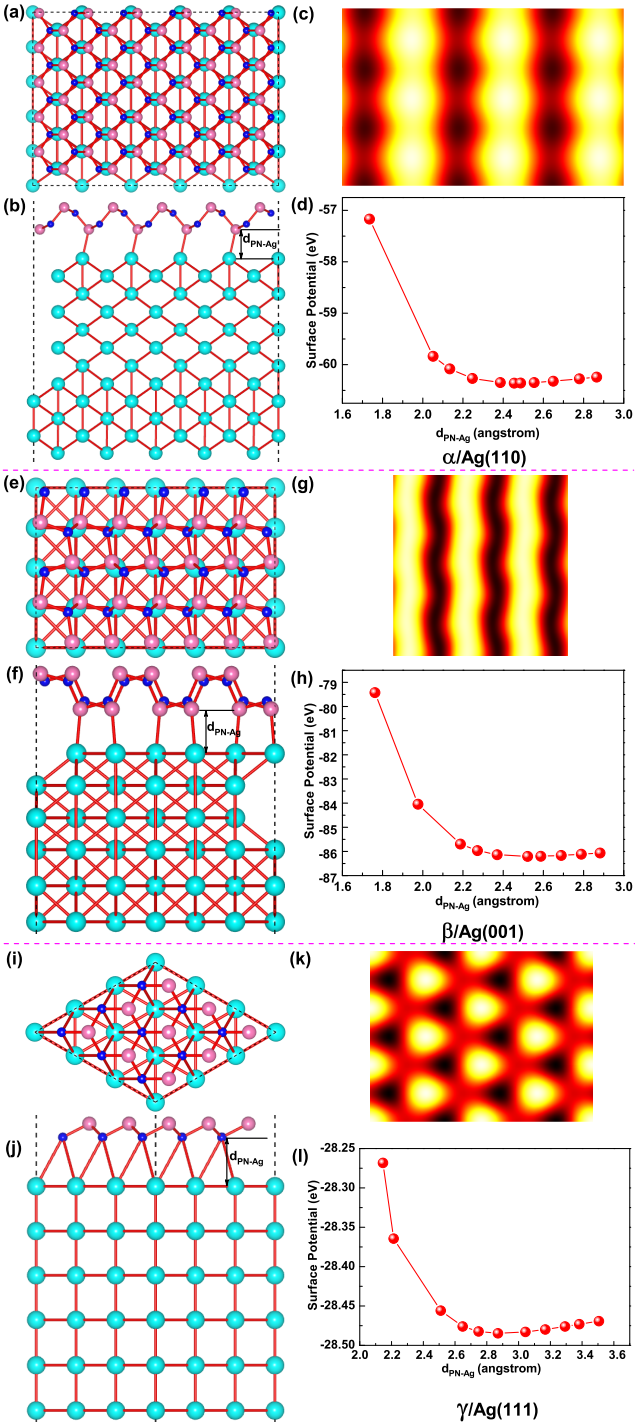

Fig. 7 (a) and (b), (e) and (f) as well as (i) and (j) stands for the top and side view of α-PN/Ag(110), β-PN/Ag(001) and γ-PN/Ag(111) system, respectively. (c), (g), and (k) are respectively the corresponding STM mapping of α-PN/Ag(110), β-PN/Ag(001) and γ-PN/Ag(111) systems under -1.0 V voltage. (d), (h) and (i) shows the surface potential of α-PN/Ag(110), β-PN/Ag(001) and γ-PN/Ag(111) systems, respectively.

N_2. The growth of the α-, β-, and γ-PN monolayer on Ag(110), Ag(001), and Ag(111), respectively are shown in Fig. 7 (a) and (b), (e) and (f), and (i) and (j), respectively. The lattice mismatch between α-PN and Ag(110) is 6.89% and 2.48% along vector $\vec{a}$ and $\vec{b}$, respectively. For γ-PN/Ag(111), the lattice-misfit is about 3.18%. The relatively small mismatch between α- and γ-PN and Ag substrates implies the potential realization of them in experiments. Although the lattice mismatch for β-PN/Ag(001) system is larger than 13%, which is a little large, we can still expect its realization similar to the growth of TiC monolayer on NiO(001) surface[49]. To better guide experiments, we further calculated surface potential (SP) between Ag substrate and the monolayer PN. The energetically favorable spacing between monolayer PN and Ag substrate is 2.455, 2.551 and 3.307 Å for α-PN/Ag(110), β-PN/Ag(001), and γ-PN/Ag(111) systems, respectively. In comparison with Boron sheet/Cu(111)[47] and silicene/Ag(111)[48] systems, the PN-Ag distances are almost greater than B-Cu and Si-Ag distances. The relative larger distance between the monolayer PN and Ag substrate indicates their weaker interaction, thereby, the PN monolayer phases may be less affected by Ag substrate. The excellent properties of the monolayer PN is hoping to be reserved under such growth condition. Meanwhile, we simulate their STM images when the monolayer grows on the Ag substrate. we only presented the corresponding STM images of the three systems at -1.0 V voltage, as shown in in Fig. 7 (c), (g) and (k), respectively, due to the results at two voltages (-1.0 and 1.0 V) are nearly the same. Obviously, the STM images clearly provide the non-planar and periodic structural characteristics of the three monolayer PN sheets as useful references for experiments.

4 Conclusions

Using first-principles calculations we predict three novel 2D phosphorus nitride (PN) monolayer sheets that can be stable under ambient pressure in contrast to previously reported 3D PN crystals. The dynamic stability of the three 2D PN even reach to high temperature under ambient pressure. The α- and γ-PN show buckled configuration while β-PN shows puckered one. The three phases are all indirect semiconductors. Their band gap and band type can be effectively modulated by multilayer stacking, in-plane strain, and 1D patterning. Particularly, the Z-αPNNRs show size-dependent ferromagnetism.

Acknowledgement

This work was financially supported by the National Natural Science Foundation of China (Grant Nos. 11574260 and

11274262) and the Natural Science Foundation of Hunan Province, China (Grand No. 14JJ2046).

References

1 K. Novoselov, D. Jiang, F. Schedin, T. Booth, V. Khotkevich, S. Morozov and A. Geim, *Proc. Natl. Acad. Sci. U.S.A*, 2005, **102**, 10451–10453.

2 K. Novoselov, A. K. Geim, S. Morozov, D. Jiang, M. Katsnelson, I. Grigorieva, S. Dubonos and A. Firsov, *Nature*, 2005, **438**, 197–200.

3 A. K. Geim and K. S. Novoselov, *Nat. Mater.*, 2007, **6**, 183–191.

4 A. C. Neto, F. Guinea, N. Peres, K. S. Novoselov and A. K. Geim, *Rev. Mod. Phys.*, 2009, **81**, 109.

5 C. Jin, F. Lin, K. Suenaga and S. Iijima, *Phys. Rev. Lett.*, 2009, **102**, 195505.

6 P. Joensen, R. Frindt and S. R. Morrison, *Mater. Res. Bull.*, 1986, **21**, 457–461.

7 S. Cahangirov, M. Topsakal, E. Aktürk, H. Şahin and S. Ciraci, *Phys. Rev. Lett.*, 2009, **102**, 236804.

8 P. De Padova, C. Quaresima, C. Ottaviani, P. M. Sheverdyaeva, P. Moras, C. Carbone, D. Topwal, B. Olivieri, A. Kara, H. Oughaddou *et al.*, *Appl. Phys. Lett.*, 2010, **96**, 261905.

9 B. Feng, Z. Ding, S. Meng, Y. Yao, X. He, P. Cheng, L. Chen and K. Wu, *Nano Lett.*, 2012, **12**, 3507–3511.

10 Y. Miyamoto and B. D. Yu, *Appl. Phys. Lett.*, 2002, **80**, 586–588.

11 A. R. Botello-Méndez, F. López-Urías, M. Terrones and H. Terrones, *Nano Lett.*, 2008, **8**, 1562–1565.

12 M. Topsakal, S. Cahangirov, E. Bekaroglu and S. Ciraci, *Phys. Rev. B*, 2009, **80**, 235119.

13 W. Wu, P. Lu, Z. Zhang and W. Guo, *ACS Appl. Mater. Interfaces*, 2011, **3**, 4787–4795.

14 A. Du, Z. Zhu, Y. Chen, G. Lu and S. C. Smith, *Chem. Phys. Lett.*, 2009, **469**, 183–185.

15 H. Şahin, S. Cahangirov, M. Topsakal, E. Bekaroglu, E. Akturk, R. T. Senger and S. Ciraci, *Phys. Rev. B*, 2009, **80**, 155453.

16 H. Li, J. Dai, J. Li, S. Zhang, J. Zhou, L. Zhang, W. Chu, D. Chen, H. Zhao, J. Yang *et al.*, *J. Phys. Chem. C*, 2010, **114**, 11390–11394.

17 H. Liu, A. T. Neal, Z. Zhu, Z. Luo, X. Xu, D. Tománek and P. D. Ye, *ACS nano*, 2014, **8**, 4033–4041.

18 J. Guan, Z. Zhu and D. Tománek, *Phys. Rev. Lett.*, 2014, **113**, 046804.

19 Z. Zhu and D. Tománek, *Phys. Rev. Lett.*, 2014, **112**, 176802.

20 M. Wu, H. Fu, L. Zhou, K. Yao and X. C. Zeng, *Nano Lett.*, 2015, **15**, 3557–3562.

21 S. Zhang, Z. Yan, Y. Li, Z. Chen and H. Zeng, *Angewandte Chemie*, 2015, **127**, 3155–3158.

22 C. Kamal and M. Ezawa, *Phys. Rev. B*, 2015, **91**, 085423.

23 J. Qiao, X. Kong, Z.-X. Hu, F. Yang and W. Ji, *Nat. Commu.*, 2014, **5**, 4475.

24 Z. Zhang, J. Xie, D. Yang, Y. Wang, M. Si and D. Xue, *Appl. Phys. Express*, 2015, **8**, 055201.

25 G. Bettermann, W. Krause, G. Riess and T. Hofmann, *Phosphorus Compounds, Inorganic. Ullmann's Encyclopedia of Industrial Chemistry.*, Wiley Online Library, 2000.

26 W. Schnick, J. Lücke and F. Krumeich, *Chem. Mater.*, 1996, **8**, 281–286.

27 Y. Yamada, N. Yoshikawa, H. Sasai and M. Shibasaki, *Angew. Chem. Int. Ed.*, 1997, **36**, 1871–1873.

28 K. Landskron, H. Huppertz, J. Senker and W. Schnick, *Angew. Chem. Int. Ed.*, 2001, **40**, 2643–2645.

29 J. Dong, A. Kinkhabwala and P. McMillan, *Phys. Status Solidi (B)*, 2004, **241**, 2319–2325.

30 P. Kroll and W. Schnick, *Chem. Eur. J.*, 2002, **8**, 3530–3537.

31 Z. Raza, I. Errea, A. R. Oganov and A. M. Saitta, *Sci. Rep.*, 2014, **4**, 5889.

32 H. Allcock, *Phosphorus-Nitrogen Compounds: Cyclic, Linear, and High Polymeric Systems*, Elsevier, 2012.

33 G. Kresse and J. Furthmüller, *Phys. Rev. B*, 1996, **54**, 11169.

34 G. Kresse and J. Furthmüller, *Comput. Mater. Sci.*, 1996, **6**, 15–50.

35 J. P. Perdew, K. Burke and M. Ernzerhof, *Phys. Rev. Lett.*, 1996, **77**, 3865.

36 P. E. Blöchl, *Phys. Rev. B*, 1994, **50**, 17953.

37 G. Kresse and D. Joubert, *Phys. Rev. B*, 1999, **59**, 1758.

38 O. Hod, V. Barone, J. E. Peralta and G. E. Scuseria, *Nano Lett.*, 2007, **7**, 2295–2299.

39 T. Dumitrică, M. Hua and B. I. Yakobson, *Phys. Rev. B*, 2004, **70**, 241303.

40 J. Gao, J. Zhang, H. Liu, Q. Zhang and J. Zhao, *Nanoscale*, 2013, **5**, 9785–9792.

41 K. Parlinski, Z. Li and Y. Kawazoe, *Phys. Rev. Lett.*, 1997, **78**, 4063.

42 J. Paier, M. Marsman, K. Hummer, G. Kresse, I. C. Gerber and J. G. Ángyán, *J. Chem. Phys.*, 2006, **124**, 154709.

43 J. Paier, M. Marsman, K. Hummer, G. Kresse, I. Gerber and J. Ángyán, *J. Chem. Phys.*, 2006, **125**, 9901.

44 G. Henkelman, A. Arnaldsson and H. Jónsson, *Comput. Mater. Sci.*, 2006, **36**, 354–360.

45 E. Sanville, S. D. Kenny, R. Smith and G. Henkelman, *J. Comp. Chem.*, 2007, **28**, 899–908.

46 J. Gao, J. Yip, J. Zhao, B. I. Yakobson and F. Ding, *J. Am. Chem. Soc.*, 2011, **133**, 5009–5015.

47 J. Gao and J. Zhao, *Sci. Rep.*, 2012, **2**, 861.

48 H. Liu, J. Gao and J. Zhao, *Sci. Rep.*, 2013, **3**, 3288.

49 Z. Zhang, X. Liu, B. I. Yakobson and W. Guo, *J. Am. Chem. Soc.*, 2012, **134**, 19326–19329.